Anisotropy of the electron spin-resonance linewidth of $CuGeO_3$

1997 J. Phys.: Condens. Matter 9 3779

(http://iopscience.iop.org/0953-8984/9/18/016)

J. Phys.: Condens. Matter **9** (1997) 3779–3792. Printed in the UK PII: S0953-8984(97)75513-9

Anisotropy of the electron spin-resonance linewidth of $CuGeO_3$

B Pilawa

Physikalisches Institut, Universität Karlsruhe (TH), POB 6980, D-76128 Karlsruhe, Germany

Received 18 June 1996, in final form 28 November 1996

Abstract. This paper presents measurements of the angular variation of the position and width of ESR lines in three mutually perpendicular planes of a single crystal of $CuGeO_3$ in the temperature range 12–200 K at two widely differing microwave frequencies. The analysis is carried out in terms of the anisotropic exchange and anisotropic Zeeman interaction. The variations of the anisotropy of the linewidth can be attributed to a temperature dependence of the orientation and the principal values of the exchange tensor.

1. Introduction

$CuGeO_3$ is a quasi-one-dimensional spin-$S = 1/2$ Heisenberg antiferromagnet ($|J_c/k_B| \approx$ 90 K [1], $J_b \approx J_c/10$ [2]), which shows at low temperatures ($T_{SP} = 14$ K) a spin–Peierls phase transition [3]. Induced by spin–phonon coupling, dimerization of the uniform spin chains takes place below T_{SP}, so the non-magnetic $S = 0$ ground state becomes separated by an energy gap from an excited $S = 1$ triplet state. In the low-temperature range, a magnetic phase transition takes place at about $B_c \approx 12$ T from the non-magnetic to a magnetic spin–Peierls phase. So far the spin–Peierls transition has only been found in organic systems [4], and since $CuGeO_3$ is the first inorganic compound found to undergo such a transition, it has been studied carefully by many experimental techniques (neutron scattering [2, 5], Raman scattering [6, 7], specific heat [8], magnetization [1, 9]). The subject of this paper is an ESR study of $CuGeO_3$.

ESR measurements allow a sensitive investigation of both the static and the dynamic properties of the Cu^{2+} spins. Oseroff *et al* [10] determined for the first time the energy gap in the dimerized spin–Peierls phase by ESR, and observed a large increase of the linewidth with increasing temperature. This was attributed to a diffusive behaviour of the spin-correlation functions, and interpreted as an indication of the excellent one-dimensional properties of $CuGeO_3$. These results were confirmed by Honda *et al* [13], who revealed, by a study of the anisotropy of the linewidth, that the line broadening is caused by the symmetric part of the anisotropic exchange interaction. Recently, these results were contradicted by Yamada *et al* [12]. They studied the ESR line up to $T = 800$ K and found that there are no indications for spin diffusion, and that both the temperature dependence and the anisotropy of the linewidth are probably caused by the antisymmetric Dzyaloshinski–Moriya exchange interaction. All of these studies were carried out at relatively low frequencies ($\nu \lesssim 35$ GHz). ESR measurements at larger frequencies were used to probe directly the energy gap of the spin–Peierls phase [11], and the spin dynamics of the non-magnetic and magnetic spin–Peierls phase [14, 15].

0953-8984/97/183779+14$19.50

Since it is important for the interpretation of ESR results to know which types of anisotropic interaction contribute to the broadening of the linewidth, measurements of the anisotropy of the ESR linewidth were carried out at low (9.5 GHz) and high frequency (245 GHz) at temperatures ranging between $T = 12$ K and 200 K. The experimental results allow an accurate characterization of the anisotropic interactions.

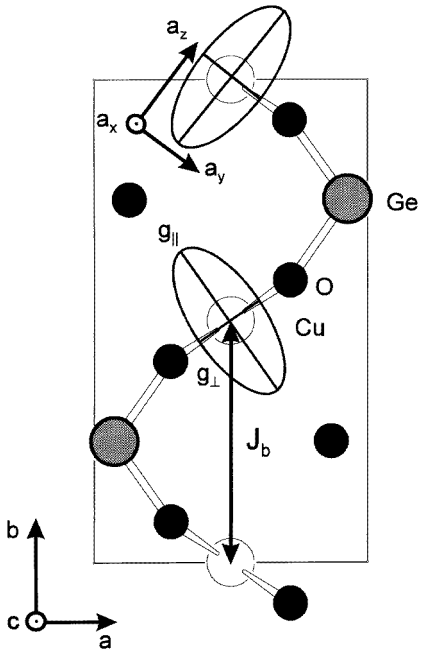

Figure 1. A view of the crystallographic unit cell of $CuGeO_3$ along the *c*-axis. The orientation of the *g*-tensor (central Cu^{2+} ion) and the principal axes of the exchange tensor $A^{(n)}_{\mu\mu}$ (upper Cu^{2+} ion) are indicated by ellipsoids.

2. Experimental details and results

ESR measurements of various samples ($\approx 2 \times 3 \times 0.5$ mm^3) were carried out at 9.5 GHz with a Bruker ESP300E spectrometer and at 245 GHz with the high-magnetic-field ESR equipment of the Grenoble High Magnetic Field Laboratory [16] in the temperature range 12–200 K. A transmission configuration (Faraday configuration) was used at 245 GHz, and three samples ($\approx 5 \times 3 \times 0.5$ mm^3) were cut from one larger crystal, in such a way that measurements of the angular dependence of the ESR signal could be carried out in the three principal planes (*ab*, *bc*, and *ca*) of the orthorhombic crystal structure of $CuGeO_3$. A view of the crystallographic unit cell along the *c*-direction is given in figure 1. With regard to the interpretation of the ESR results, it is important to note that there are two magnetically inequivalent Cu^{2+} sites. There are two kinds of strongly exchange-coupled copper chains running along the *c*-direction [17]. The ESR line shapes observed at 9.5 GHz are Lorentzian. At 245 GHz the resonance lines are distorted in many cases by reflections of the microwaves in the transmission line as well as by a mixing of the absorption and dispersion signal. These effects are hard to control, and change from one experiment to

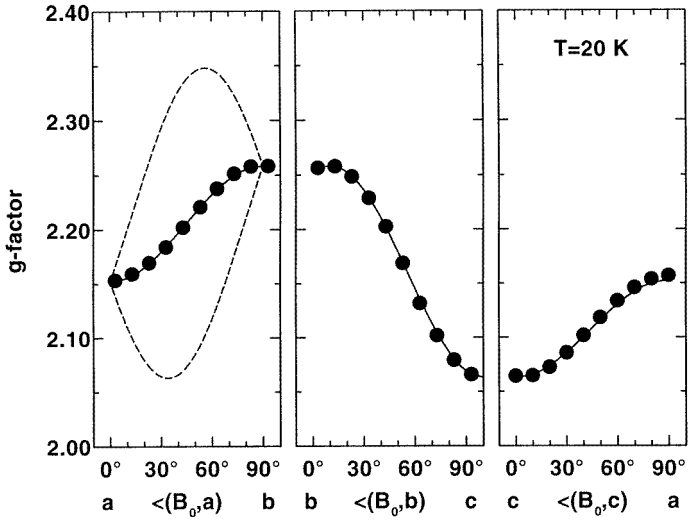

Figure 2. The angular variation of the g-factor in the crystallographic ab-, bc-, and ca-planes of $CuGeO_3$ at 20 K. The solid line shows the fit with the principal g-values given in the text. The broken lines indicate the variation of the g-factor of the two magnetically inequivalent chains.

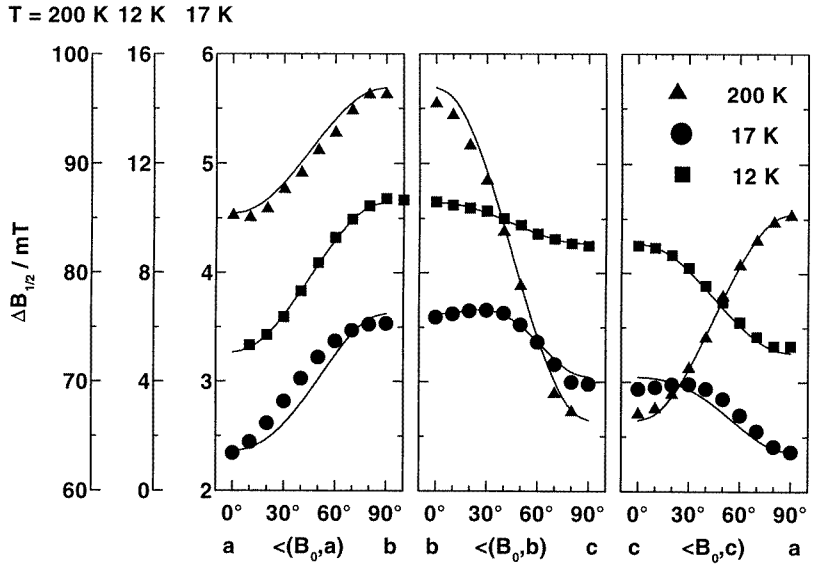

Figure 3. The anisotropy of the ESR linewidth at 9.5 GHz. Dots: experimental results; solid lines: the calculated anisotropy of the ESR linewidth (for details, see the text).

another in an unpredictable manner. Therefore the width of the resonance is sometimes not well defined. The errors due to theses effects are about 10% of $\Delta B_{1/2}$.

The experimental results are shown in figures 2, 3, and 4. Figure 2 shows the angular variation of the g-factor at 20 K. In agreement with earlier measurements, the g-factor is nearly temperature independent. Figures 3 and 4 show the anisotropy of the linewidth for

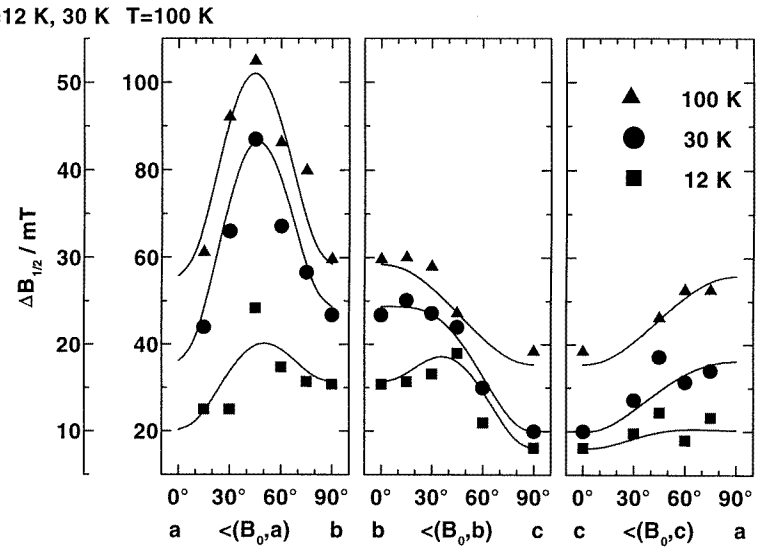

Figure 4. The anisotropy of the ESR linewidth at 245 GHz. Dots: experimental results; solid lines: the calculated anisotropy of the ESR linewidth (for details, see the text).

9.5 GHz and 245 GHz, respectively. At 9.5 GHz the size of the linewidth decreases from large values at high temperatures ($\Delta B_{1/2} > 100$ mT) down to $\Delta B_{1/2} \approx 6$ mT at 30 K, without any significant change of the anisotropy of $\Delta B_{1/2}$. However, below $T \approx 30$ K very characteristic changes of the anisotropy of $\Delta B_{1/2}$ are observed. The minimum of the linewidth shifts from the crystallographic c-direction to the a-direction, and an additional peak develops just above the spin–Peierls phase transition in the bc-plane. A large maximum of the linewidth is found in the ab-plane for measurements at 245 GHz. As for the measurements at 9.5 GHz, a small peak develops at low temperatures in the bc-plane.

3. Discussion of the experimental results

The linewidth of the Lorentzian-shaped ESR absorptions is given by the integral

$$\Delta B_{1/2} = \frac{\hbar}{g\mu_B} \mathrm{Re} \int_0^\infty \mathrm{d}\tau \ \Psi(\tau). \tag{1}$$

of the relaxation function

$$\Psi(\tau) = \frac{1}{\hbar^2} \frac{\langle [\hat{H}_A(\tau), \hat{S}^+][\hat{S}^-, \hat{H}_A] \rangle}{\langle \hat{S}^+ \hat{S}^- \rangle} \tag{2}$$

where the $\hat{S}^\pm$ denote transverse components of the total spin and of the exchange-coupled spins, $\langle\ \rangle$ denotes the thermal average, and $\hat{H}_A$ denotes the Hamiltonian of the anisotropic spin–spin coupling [18–20]. In order to estimate the contributions of the various anisotropic interactions, the integral can be approximated by

$$\Delta B_{1/2} \approx \frac{\hbar}{g\mu_B} \Psi(0) \tau_c \tag{3}$$

with the second moment $M_2^{(A)} = \Psi(0)$, and the correlation time $\tau_c \approx (|J|/\hbar)^{-1}$. When the second moments are simply estimated as the squares of the parameters of the corresponding

spin-Hamiltonian parameters, the ESR linewidth due to the hyperfine interaction of the electron with the nuclear spin of the copper ions is in the range $\Delta B_{1/2} \approx (A_{||})^2/\gamma_e\overline{h}|J_c| \approx 5\ \mu$T, with $A_{||} = g_{Cu}\beta_{Cu} \times 43.6$ T and $\gamma_e = g\mu_B/\overline{h} = 1.76 \times 10^{11}$ rad s^{-1} T^{-1}. The linewidth due to the magnetic dipole–dipole interaction is $\Delta B_{1/2} \approx (\omega_d)^2/\gamma_e(|J_c|/\overline{h}) \approx 0.1$ mT, with $\omega_d = (\mu_0/4\pi)\overline{h}\gamma_e^2/c^3$ and $c = 2.941$ Å. The comparison with the experimental results shows that these two contributions are of minor importance. The most important contributions to the ESR linewidth can be expected for the anisotropic exchange interaction $\hat{H}_{AE}$:

$$\Delta B_{1/2} \approx \frac{1}{\gamma_e}\frac{(A_z)^2}{|J_c|\overline{h}} \approx 23 \text{ mT}$$

with $A_z \approx (\Delta g/g)^2|J_c|$ [22] and $\Delta g/g \approx 0.174$, and for the anisotropic Zeeman interaction $\hat{H}_{AZ}$:

$$\Delta B_{1/2} \approx \frac{1}{\gamma_e}\frac{(g\mu_B B_0)^2}{|J_c|\overline{h}}\left(\frac{\Delta g}{g}\right)^2 \approx 35 \text{ mT}$$

in strong magnetic fields ($B_0 \approx 8.7$ T).

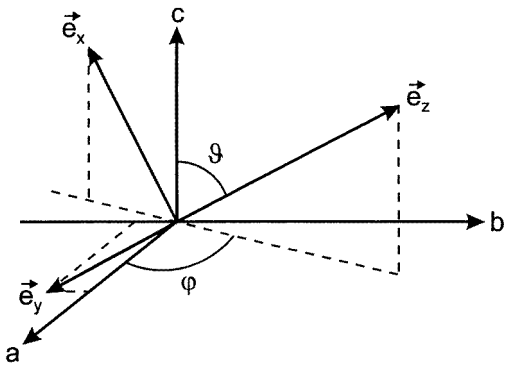

Figure 5. Crystallographic *a*-, *b*-, *c*- and laboratory e_x-, e_y-, e_z-coordinates used for the mathematical description of the ESR. The B_0-field is applied parallel to the z-direction.

In the following, the analysis of the anisotropy of the linewidth will be discussed in terms of the anisotropic exchange and Zeeman interaction.

3.1. The anisotropic exchange interaction

The analysis of the ESR measurements at 9.5 GHz is carried out in terms of the symmetric part of the anisotropic exchange interaction $\hat{H}_{AE}$. Like the magnetic dipole–dipole interaction, the Hamiltonian of the anisotropic exchange interaction is given by the sum

$$\hat{H}_{AE} = \sum_{M=-2}^{2} \hat{G}_M \tag{4}$$

with

$$\hat{G}_0 = \sum_{i \neq j} \frac{1}{4} A_0(ij)(3\hat{s}_i^z\hat{s}_j^z - \hat{\boldsymbol{s}}_i \cdot \hat{\boldsymbol{s}}_j)$$

$$\hat{G}_{\pm 1} = \sum_{i \neq j} -\frac{3}{4} A_{\pm 1}(ij)(\hat{s}_i^{\pm}\hat{s}_j^z + \hat{s}_j^{\pm}\hat{s}_i^z)$$

and

$$\hat{G}_{\pm 2} = \sum_{i \neq j} -\frac{3}{8} A_{\pm 2}(ij) \hat{s}_i^{\pm} \hat{s}_j^{\pm}.$$

The A_t ($t = 0, \pm 1, \pm 2$) denote the geometrical parameters of the anisotropic exchange, and $\hat{s}_i$ the individual spins. The coordinates x, y, z refer to a coordinate system in which the z-direction is defined by the direction of the applied magnetic field $\boldsymbol{B}_0$ (compare figure 5). When only nearest-neighbour interactions are considered, equations (1) and (4) lead to (mathematical details are given in the appendix)

$$\Delta B_{1/2} = \frac{1}{\gamma_e} \frac{9}{4\overline{h}^2} \mathrm{Re}(|A_0|^2 f_0 + |A_1|^2 f_1 + |A_2|^2 f_2). \tag{5}$$

f_0, f_1, and f_2 denote spectral densities, which at least at high temperature are in the ratio 1:10:1. In order to fit the experimental data, the spectral densities are used as parameters.

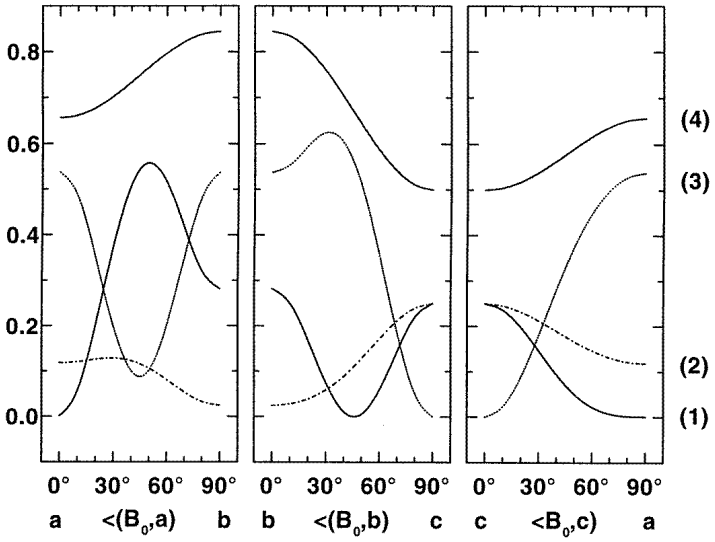

Figure 6. Curves 1, 2 and 3 show the angular variation of the geometrical factors $|A_0/A_z|^2$, $|A_2/A_z|^2$ and $10|A_1/A_z|^2$ of the symmetric part of the anisotropic exchange. Curve 4 shows $(|A_0|^2 + 10|A_1|^2 + |A_2|^2)/(A_z)^2$. The curves are calculated for $\alpha = -1/2$, and $\angle(\boldsymbol{a}_z, \boldsymbol{a}) = 56^\circ$.

Table 1. Parameters for fitting the anisotropy of the linewidth at 9.5 GHz. α denotes the orthorhombic distortion of the exchange tensor, $\angle(\boldsymbol{a}_z, \boldsymbol{a})$ the angle between the a_z-axis and the crystallographic a-direction (see figure 1). $\Delta B_0 = (1/\gamma_e)(3A_z/2\overline{h})^2 f_0$ is used as a scaling parameter, $f_0{:}f_1{:}f_2$ is the ratio of the spin-correlation functions of table 3 (see later).

T/K	$\lvert\alpha\rvert$	$\angle(\boldsymbol{a}_z, \boldsymbol{a})$	ΔB_0/mT	$f_0{:}f_1{:}f_2$
200	0.55 ± 0.01	$(50 \pm 1)^\circ$	124 ± 2	1:10:1
100	0.57 ± 0.01	$(48 \pm 1)^\circ$	60 ± 1	1:10:1
30	0.61 ± 0.02	$(48 \pm 1)^\circ$	7.9 ± 0.1	1:10:1
17	0.77 ± 0.03	$(60 \pm 1)^\circ$	4.0 ± 0.2	$1{:}(11 \pm 0.3){:}1$
12	0.83 ± 0.02	$(71 \pm 3)^\circ$	10.8 ± 0.2	1:10:1

The geometrical factors $|A_t|^2$ can be calculated from the principal values of the exchange tensor $A_x = \alpha A_z$ and $A_y = -(1+\alpha)A_z$, and the orientation of its principal axis within the unit cell. Due to the crystallographic symmetry, one of the principal axes should be parallel to the c-direction. In order to fit the experimental data, the orthorhombic distortion α and the angle of the z-axis to the a-direction of the exchange tensor (compare figure 1) are used as fitting parameters. The solid lines of figure 3 are calculated with the parameters given in table 1.

Figure 6 shows the angular variation of the $|A_t|^2$, when the magnetic field is applied in the crystallographic ab-, bc-, and ca-planes. The three contributions, $|A_0|^2$, $|A_1|^2$, and $|A_2|^2$, can be clearly distinguished by their angular variations, so deviations of $f_0{:}f_1{:}f_2$ from the ratio 1:10:1 should lead to characteristic changes in the anisotropy of the ESR linewidth. Nearly all of the measurements carried out at 9.5 GHz give no indication that this ratio should be changed. Only the measurements just above the spin–Peierls phase transition demand a slight increase of f_1 due to the additional peak observed in the bc-plane. Although nearly no temperature dependence in the ratio of the spectral densities could be detected, the anisotropy of $\Delta B_{1/2}$ reveals a temperature dependence of the orientation and the size of the orthorhombic distortion of the exchange tensor (compare table 1). In agreement with previous findings [21], this anisotropy is very small at high temperatures, but it becomes considerable just above and below the spin–Peierls transition. The temperature dependence of the exchange tensor may be caused by the temperature dependence of the lattice parameters.

3.2. The anisotropic Zeeman interaction

The anisotropic Zeeman interaction becomes important for the analysis of ESR measurements on $CuGeO_3$ in high magnetic fields, due to the anisotropic g-tensor of the Cu^{2+} ions. Figure 1 shows the difference in the orientation of the g-tensors of neighbouring Cu^{2+} ions along the b-direction. Therefore two resonance signals at quite different magnetic fields B_0 should be observed when the field is applied in the ab-plane. However, due to the strong exchange coupling J_b along the b-direction only one resonance can be observed. Therefore it can be expected that the linewidth should increase with increasing magnetic field strength, due to the increasing ratio between the difference $B_0^{(1)} - B_0^{(2)}$ of the resonance fields of the two kinds of spin and $|J_b|$. This is the reason for the additional peak in the anisotropy of the linewidth in the ab-plane observed for the measurement at 245 GHz (compare figure 4).

The additional contribution of this Zeeman broadening of the linewidth can be calculated in the framework of the theory of exchange narrowing and averaging. The calculation carried out in the appendix (equations (A9)–(A19)) gives the following expression (compare also [23]):

$$\Delta B_{1/2} = \frac{1}{\gamma_e}\frac{(\mu_B B_0)^2}{\hbar|J_b|}\sqrt{\frac{\pi}{8}}\,\mathrm{Re}\left(|\Delta g_{zz}|^2 + |\Delta g_{zx} + \mathrm{i}\,\Delta g_{zy}|^2\frac{1}{2}\exp\left[-\frac{1}{8}(\hbar\omega_0/J_b)^2\right]\right). \tag{6}$$

It turns out that the linewidth is proportional to the square of the resonance field B_0, and the squares of the difference between the g-tensors of the two kinds of spin, $\Delta g_{z\mu} = \frac{1}{2}(g_{z\mu}^{(1)} - g_{z\mu}^{(2)})$, $\mu = x, y, z$.

The local g-tensors of the Cu^{2+} ions are well defined by the anisotropy of the g-factor shown in figure 2. The crystallographic symmetry of the nearest neighbourhood of the Cu^{2+} ions is nearly tetragonal, so the ground state of the Cu^{2+} ions is a $d_{x^2-y^2}$ orbital, which is characterized by an axial g-tensor, with a large value of $g_{||}$ perpendicular to the plane

of the neighbouring oxygen atoms and a smaller value of $g_\perp$ in the plane (figure 1). The orientation and the principal values of the g-tensors can be determined from the angular variation of the resonance field strength B_0 via

$$\omega_0 = \bar{g}\mu_B B_0/\bar{h} \tag{7}$$

with $\bar{g} = \sqrt{\bar{g}_{zx}^2 + \bar{g}_{zy}^2 + \bar{g}_{zz}^2}$. The comparison between the experimental results at 20 K and equation (7) is shown in figure 2. The solid line is calculated with the principal g-factors $g_{\|} = 2.348 \pm 0.005$ and $g_\perp = 2.063 \pm 0.005$. The principal axis of the g-tensor is perpendicular to the c-direction. The angles with respect to the a-direction are 56° and 124° for the two Cu^{2+} sites, respectively.

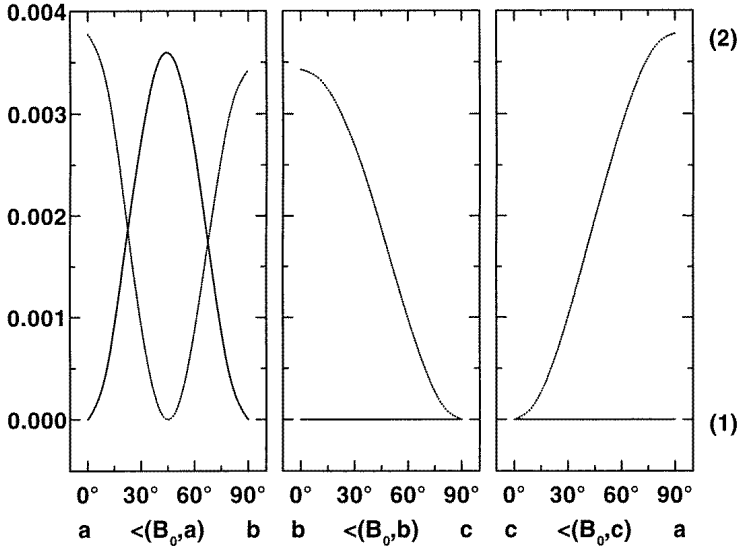

Figure 7. Curve 1: the angular variation of $|\Delta g_{zz}/\bar{g}|^2$; curve 2: the angular variation of $|\Delta(g_{zx} + \mathrm{i}\,\Delta g_{zy})/\bar{g}|^2$.

The important result of equation (6) is that, within the approximations made in the appendix, the contribution of the anisotropic Zeeman interaction to the ESR linewidth is only determined by the inter-chain exchange J_b. Therefore J_b is used as a parameter to fit the experimental result.

Table 2. Parameters for fitting the anisotropy of the linewidth at 245 GHz. The notation is as in table 1.

T/K	$\|\alpha\|$	$\angle(\boldsymbol{a}_z, \boldsymbol{a})$	ΔB_0/mT	$f_0{:}f_1{:}f_2$	$\bar{h}\omega_0/\|J_b\|$
100	0.57 ± 0.01	(48 ± 1)	64 ± 4	1:10:1	2.8 ± 0.3
30	0.77 ± 0.6	(70 ± 7)	13 ± 2	$1{:}(13 \pm 2){:}1$	1.65 ± 0.1
20	0.77 ± 0.6	(70 ± 7)	10.5 ± 1	$1{:}(15 \pm 2){:}1$	1.1 ± 0.1
12	0.77 ± 0.6	(70 ± 7)	10.5 ± 1	$1{:}(17 \pm 2){:}1$	0.5 ± 0.1

Figure 7 shows the angular variation of $|\Delta g_{zz}/\bar{g}|^2$ and $|(\Delta g_{zx} + \mathrm{i}\,\Delta g_{zy})/\bar{g}|^2$, which determines the anisotropy of the Zeeman contribution to the ESR linewidth. The anisotropy

of the linewidth at 245 GHz is calculated including the combined contributions of the anisotropic exchange and Zeeman interactions. The parameters used to calculate the solid lines in figure 4 are given in table 2. With the ratio $\hbar\omega_0/|J_b| = 2.8$ used to adjust the Zeeman contribution at $T = 100$ K, the inter-chain exchange constant becomes $|J_b/k_B| \approx 4.2$ K, which is in reasonable agreement with $|J_b| \approx |J_c/10|$ observed in neutron scattering experiments [2]. At lower temperatures the decreasing ratio $\hbar\omega_0/|J_b|$ shows the breakdown of the Gaussian approximation for the spectral density. In contrast to the measurements at 9.5 GHz, the ratio $f_0{:}f_1{:}f_2$ for the anisotropic exchange changes continuously from 1:10:1 at high temperatures to 1:17:1 at $T = 12$ K, which indicates the influence of the magnetic field on the spectral densities of the spin-correlation functions.

4. Conclusion

The anisotropy of the ESR linewidth is measured at 9.5 and 245 GHz between 12 K and 200 K, and it is shown that a description of the observed anisotropy of the ESR linewidth is possible in terms of the anisotropic exchange and Zeeman interaction.

The angular variation of $\Delta B_{1/2}$ reveals an orthorhombic distortion of the exchange tensor, which shows a characteristic temperature dependence. In agreement with previous findings for the exchange tensor [22], this anisotropy is very small at high temperatures, but it becomes considerable just above and below the spin–Peierls transition. The principal axes of the exchange tensor are only roughly determined by the orientation of the g-tensor. As for the anisotropy of the exchange tensor, the orientation of the principal axes depends on temperature, especially in the range of the spin–Peierls transition. The temperature dependence of the exchange tensor may be caused by the temperature dependence of the lattice parameters.

The anisotropic Zeeman interaction becomes important for the analysis of ESR measurements on $CuGeO_3$ in high magnetic fields, due to the fact that there are two magnetically different types of spin chain. The broadening of the ESR line by the Zeeman interaction is narrowed only by the weak inter-chain exchange J_b and not by the strong intra-chain exchange J_c, like for the anisotropic exchange. Therefore the broadening of the ESR line by the anisotropic Zeeman interaction is at least a factor of 10 more effective than the broadening by the anisotropic exchange.

An important consequence for ESR studies of $CuGeO_3$ in high magnetic fields is that the linewidth contains information on the four spin-correlation functions related to the anisotropic exchange and the two spin-correlation functions of the anisotropic Zeeman interaction. By altering the direction of the applied magnetic field, it is possible to study either the transverse ($\boldsymbol{B}_0||\boldsymbol{a}$ or $\boldsymbol{b}$), or the longitudinal components of the two spin-correlation functions ($\boldsymbol{B}_0 \perp \boldsymbol{c}$ and $\angle(\boldsymbol{B}_0, \boldsymbol{a}) = 45^\circ$). For $\boldsymbol{B}_0||\boldsymbol{c}$ the Zeeman broadening is completely suppressed.

Acknowledgments

I would like to thank J P Boucher for many useful discussions. I would like also to thank J Wosnitza and J P Boucher for providing the samples studied, which were prepared by R K Kremer and A Revcolevschi, respectively. This work was supported by the Human Capital and Mobility Programme of the European Community.

Appendix

Kubo showed that the width of exchange-narrowed Lorentzian resonance lines is given by the integral [18, 19]

$$\Delta B_{1/2} = \frac{1}{\gamma_e}\mathrm{Re}\int_0^\infty \mathrm{d}\tau\ \Psi(\tau) \tag{A1}$$

of the relaxation function

$$\Psi(\tau) = \frac{1}{\hbar^2}\frac{\langle[\hat{H}_A(\tau), \hat{S}^+][\hat{S}^-, \hat{H}_A]\rangle}{\langle\hat{S}^+\hat{S}^-\rangle}. \tag{A2}$$

where $\langle\ \rangle$ denotes the thermal average, the $\hat{S}^\pm$ are the transverse components of the total spin, and $\hat{H}_A$ is the anisotropic spin–spin interaction, which broadens the resonance. The time development of $\hat{H}_A$ is calculated in the interaction representation according to

$$\hat{H}_A(t) = \mathrm{e}^{-\mathrm{i}\hat{H}_0 t/\hbar}\hat{H}_A\mathrm{e}^{\mathrm{i}\hat{H}_0 t/\hbar} \tag{A3}$$

where $\hat{H}_0$ is the sum of the isotropic Zeeman ($\hat{H}_Z$) and the exchange ($\hat{H}_{ex}$) interactions. Since $\hat{H}_Z$ commutes with $\hat{H}_{ex}$, the Hamiltonian $\hat{H}_A(t)$ can be rewritten as

$$\hat{H}_A(t) = \sum_M \mathrm{e}^{\mathrm{i}M\omega_0 t}\hat{G}_M(t) \qquad \text{with } \hat{G}_M(t) = \mathrm{e}^{-\mathrm{i}\hat{H}_{ex}t/\hbar}\hat{G}_M\mathrm{e}^{\mathrm{i}\hat{H}_{ex}t/\hbar}. \tag{A4}$$

With the abbreviation $\hat{g}_M = [\hat{G}_M, \hat{S}^+]$, and since $\hat{H}_{ex}$ commutes with the components of the total spin, $[\hat{G}_M(t), \hat{S}^+]$ becomes $\hat{g}_M(t) = \mathrm{e}^{-\mathrm{i}\hat{H}_{ex}t/\hbar}[\hat{G}_M, S^+]\mathrm{e}^{\mathrm{i}\hat{H}_{ex}t/\hbar}$, so the relaxation function simplifies to

$$\Psi(t) = \frac{1}{\hbar^2}\sum_M (\langle\hat{g}_M(t)\hat{g}_M^*\rangle\mathrm{e}^{\mathrm{i}M\omega_0 t})\Big/\langle\hat{S}^+\hat{S}^-\rangle. \tag{A5}$$

In the following, the ESR linewidths according to equations (A1) and (A5) are calculated for the anisotropic exchange and the anisotropic Zeeman interactions.

Table A1. The operators $\hat{g}_M$ of the symmetric anisotropic exchange $\hat{H}_{AE}$ and the anisotropic Zeeman Hamiltonian $\hat{H}_{AZ}$ (for details, see the text).

M	$\hat{g}_M$ of $\hat{H}_{AE}$	$\hat{g}_M$ of $\hat{H}_{AZ}$
0	$\sum_{i\neq j}\frac{3}{2}A_0(ij)\hat{s}_i^z\hat{s}_j^+$	$\mu_B B_0\sum_{i\in 1}\sum_{j\in 2} g_{zz}(\hat{s}_i^+ - \hat{s}_j^+)$
+1	$\sum_{i\neq j}-\frac{3}{2}A_1(ij)\hat{s}_i^+\hat{s}_j^+$	0
−1	$\sum_{i\neq j}-\frac{3}{2}A_{-1}(ij)(\hat{s}_i^-\hat{s}_j^+ - 2\hat{s}_i^z\hat{s}_j^z)$	$\mu_B B_0\sum_{i\in 1}\sum_{j\in 2}(g_{zx} + \mathrm{i}g_{zy})(\hat{s}_i^z - \hat{s}_j^z)$
+2	0	
−2	$\sum_{i\neq j}\frac{3}{2}A_2(ij)\hat{s}_i^-\hat{s}_j^z$	

A1. The anisotropic exchange interaction

When only nearest-neighbour interactions are considered, the anisotropic exchange Hamiltonian is given by

$$\begin{aligned}\hat{H}_{AE} &= \frac{1}{2}\sum_{i,j=i\pm1}\sum_{\mu,\mu=x,y,z} A_{\mu\mu}\hat{s}_i^{\mu}\hat{s}_j^{\mu} \\ &= \sum_{i,j=i\pm1}\frac{1}{4}A_0(3\hat{s}_i^z\hat{s}_j^z - \hat{\boldsymbol{s}}_i\cdot\hat{\boldsymbol{s}}_j) - \sum_{i,j=i\pm1}\frac{3}{4}A_+(\hat{s}_i^+\hat{s}_j^z + \hat{s}_j^+\hat{s}_i^z) + \text{CC} \\ &\quad - \sum_{i,j=i\pm1}\frac{3}{8}A_{+2}\hat{s}_i^+\hat{s}_j^+ + \text{CC} \\ &= \sum_{M=-2}^{+2}\hat{G}_M\end{aligned} \tag{A6}$$

with

$$A_0 = A_{zz} \qquad A_{\pm1} = -\frac{1}{3}(A_{xz} \mp \mathrm{i}A_{yz}) \qquad A_{\pm2} = -\frac{1}{3}(A_{xx} - A_{yy} \mp 2\mathrm{i}A_{xy}). \tag{A7}$$

The operators $\hat{g}_M$ corresponding to $\hat{H}_{AE}$ are given in table A1, and the linewidth becomes

$$\Delta B_{1/2} = \frac{1}{\gamma_e}\frac{9}{4\hbar^2}\mathrm{Re}(|A_0|^2 f_0 + |A_1|^2 f_1 + |A_2|^2 f_2) \tag{A8}$$

with the spectral densities f_t of table A2. Equation (A8) is used for the analysis of the experiment.

Table A2. The combination of the spin-correlation functions $f_{ijkl}^{\alpha\beta}(\omega) = \int_0^\infty \mathrm{d}t\, \mathrm{e}^{\mathrm{i}\omega t} f_{ijkl}^{\alpha\beta}(t)$ with $f_{ijkl}^{\alpha\beta}(t) = \langle \hat{s}_i^{\alpha}(t)\hat{s}_j^{\beta}(t)(\hat{s}_k^{\alpha}\hat{s}_l^{\beta})^+\rangle$ for $\hat{H}_{AE}$ and $f_{nm}^{\alpha}(\omega) = \int_0^\infty \mathrm{d}t\, \mathrm{e}^{\mathrm{i}\omega t} f_{nm}^{\alpha}(t)$ with $f_{nm}^{\alpha}(t) = \langle \sum_{i\in n}\hat{s}_i^{\alpha}(t)(\sum_{j\in m}\hat{s}_j^{\alpha})^+\rangle$ for $\hat{H}_{AZ}$.

$\hat{H}_{AE}$
$f_0 = \dfrac{1}{\langle \hat{S}^+\hat{S}^-\rangle}\displaystyle\sum_{i,j=i\pm1}\sum_{k,l=k\pm1} f_{ijkl}^{z+}(0)$
$f_1 = \dfrac{1}{\langle \hat{S}^+\hat{S}^-\rangle}\displaystyle\sum_{i,j=i\pm1}\sum_{k,l=k\pm1} f_{ijkl}^{++}(-\omega_0) + f_{ijkl}^{-+}(\omega_0) + 4f_{ijkl}^{zz}(\omega_0)$
$f_2 = \dfrac{1}{\langle \hat{S}^+\hat{S}^-\rangle}\displaystyle\sum_{i,j=i\pm1}\sum_{k,l=k\pm1} f_{ijkl}^{-z}(2\omega_0)$
$\hat{H}_{AZ}$
$f_0 = \dfrac{1}{\langle \hat{S}^+\hat{S}^-\rangle}(f_{11}^{+}(0) + f_{22}^{+}(0) - f_{12}^{+}(0) - f_{21}^{+}(0))$
$f_1 = \dfrac{1}{\langle \hat{S}^+\hat{S}^-\rangle}(f_{11}^{z}(\omega_0) + f_{22}^{z}(\omega_0) - f_{12}^{z}(\omega_0) - f_{21}^{z}(\omega_0))$

A2. The anisotropic Zeeman interaction

In $CuGeO_3$ there are two kinds of Cu^{2+} ion, which are distinguished by their different orientations of the g-tensor, and the Zeeman Hamiltonian is given by

$$\hat{H}_Z = \mu_B B_0 \sum_{\mu=x,y,z} g_{z\mu}^{(1)}\sum_{i\in1}\hat{s}_i^{\mu} + \mu_B B_0 \sum_{\mu=x,y,z} g_{z\mu}^{(2)}\sum_{i\in2}\hat{s}_i^{\mu}. \tag{A9}$$

The sums $\sum_{i\in 1}$ and $\sum_{i\in 2}$ run over all spins of kind 1 and kind 2, respectively. The magnetic field is applied along the z-direction. Equation (A9) can be rearranged in the following way:

$$\hat{H}_Z = \mu_B B_0 \sum_{\mu=x,y,z} \frac{1}{2}(g_{z\mu}^{(1)} + g_{z\mu}^{(2)}) \sum_{i\in 1,2} \hat{s}_i^{\mu} + \mu_B B_0 \sum_{\mu=x,y,z} \frac{1}{2}(g_{z\mu}^{(1)} - g_{z\mu}^{(2)}) \left(\sum_{i\in 1} \hat{s}_i^{\mu} - \sum_{j\in 2} \hat{s}_j^{\mu} \right). \tag{A10}$$

The first term on the right-hand side gives the usual Zeeman operator, which defines the position of the resonance line. The second term contains the difference between the g-tensors of site one and site two, $\Delta g_{z\mu} = \frac{1}{2}(g_{z\mu}^{(1)} - g_{z\mu}^{(2)})$, and determines the Zeeman contribution to the anisotropy of the ESR linewidth. The operators $\hat{g}_M$ of the anisotropic Zeeman interaction

$$\hat{H}_{AZ} = \mu_B B_0 \sum_{i\in 1} \sum_{j\in 2} g_{zz}(\hat{s}_i^z - \hat{s}_j^z) + \frac{1}{2}\mu_B B_0 \sum_{i\in 1} \sum_{j\in 2} (g_{zx} - \mathrm{i}g_{zy})(\hat{s}_i^+ - \hat{s}_j^+) + \mathrm{CC} \tag{A11}$$

are given in table A1. And the linewidth becomes, according to equation (A5),

$$\Delta B_{1/2} = \frac{1}{\gamma_e}(\mu_B B_0)^2 \,\mathrm{Re}(\Delta g_{zz}^2 f_0 + |\Delta g_{zx} + \mathrm{i}\,\Delta g_{zy}|^2 f_1). \tag{A12}$$

The spectral densities f_t are given in table A2.

It is useful for the interpretation of the experiment to carry out a simplified calculation of the spin-correlation functions

$$f_{nm}^{\alpha}(t) = \left\langle \sum_{i\in n} \hat{s}_i^{\alpha}(t) (\sum_{j\in m} \hat{s}_j^{\alpha})^+ \right\rangle.$$

The first approximation is to neglect all of the inter-spin correlations $\langle \hat{s}_i^{\alpha}(t)(\hat{s}_j^{\alpha})^+ \rangle = 0,\ i \neq j$. Therefore only the functions $f_{11}^{\alpha}(t)$ and $f_{22}^{\alpha}(t)$ contribute. In the following the calculation of the correlation function

$$f_{11}^z(t) = \left\langle \sum_{i\in 1} \hat{s}_i^z(t) \left(\sum_{j\in 1} \hat{s}_j^z \right)^+ \right\rangle$$

is explicitly considered. The exchange Hamiltonian can be divided into parts, which act only on spins of kind 1: $\hat{H}_{ex}^{(11)}$, on spins of kind 2: $\hat{H}_{ex}^{(22)}$, or between the spins of kind 1 and kind 2: $\hat{H}_{ex}^{(12)}$. The motion of $\sum_{i\in 1} \hat{s}_i^z(t)$ is only caused by

$$\hat{H}_{ex}^{(12)} = 2 \sum_{i\in 1} \sum_{j\in 2} J_{ij}^{(12)} \hat{\mathbf{s}}_i \cdot \hat{\mathbf{s}}_j$$

since

$$\begin{aligned} &\left[\hat{H}_{ex}^{(11)}, \sum_{m\in 1} \hat{s}_m^z \right] = 0 \qquad \left[\hat{H}_{ex}^{(22)}, \sum_{m\in 1} \hat{s}_m^z \right] = 0 \\ &\left[\hat{H}_{ex}^{(12)}, \sum_{m\in 1} \hat{s}_m^z \right] = \sum_{m\in 1} \sum_{j\in 2} J_{mj}^{(12)} (\hat{s}_j^+ \hat{s}_m^- - \hat{s}_m^+ \hat{s}_j^-). \end{aligned} \tag{A13}$$

Then for short times the following expansion holds:

$$f_{11}^z(t) = \left\langle \sum_{i\in 1} \hat{s}_i^z(t) \sum_{j\in 1} \hat{s}_j^z \right\rangle \approx \left\langle \sum_{i\in 1} \hat{s}_i^z \sum_{j\in 1} \hat{s}_j^z \right\rangle - \frac{1}{2}\frac{t^2}{\hbar^2} \left\langle \left[\hat{H}_{ex}^{(12)}, \sum_{i\in 1} \hat{s}_i^z \right] \left[\sum_{i\in 1} \hat{s}_j^z, \hat{H}_{ex}^{(12)} \right] \right\rangle \tag{A14}$$

and, with equation (A13),

$$f_{11}^z(t) \approx \sum_{i\in 1} \langle \hat{s}_i^z \hat{s}_i^z \rangle - \frac{t^2}{\overline{h}^2} \sum_{i\in 1} \sum_{j\in 2} (J_{ij}^{(12)})^2 \langle \hat{s}_i^+ \hat{s}_i^- \rangle \langle \hat{s}_j^+ \hat{s}_j^- \rangle. \tag{A15}$$

With $\langle \hat{s}_i^z \hat{s}_i^z \rangle = \frac{1}{3}s(s+1) = \frac{1}{4}$ and $\langle \hat{s}_i^+ \hat{s}_i^- \rangle = \frac{2}{3}s(s+1) = \frac{1}{2}$, one gets

$$f_{11}^z(t) \approx (N/2)\frac{1}{4}\left(1 - \frac{t^2}{\overline{h}^2} \sum_{j\in 2} (J_{i\in 1 j}^{(12)})^2\right)$$

which may be extended to a Gaussian function:

$$f_{11}^z(t) \approx (N/2)\frac{1}{4} \exp\left(-\frac{t^2}{\overline{h}^2} \sum_{j\in 2} (J_{i\in 1 j}^{(12)})^2\right) \tag{A16}$$

For $CuGeO_3$, each spin of kind 1 has two neighbours of kind 2 coupled via J_b:

$$f_{11}^z(t) \approx (N/2)\frac{1}{4} \exp\left(-\frac{t^2}{\overline{h}^2} 2(J_b)^2\right). \tag{A17}$$

With $\langle \hat{S}^+ \hat{S}^- \rangle = \frac{2}{3}Ns(s+1) = \frac{1}{2}N$, the spectral densities f_0 and f_1 are

$$f_0 \approx \frac{1}{|J_b/\overline{h}|}\sqrt{\frac{\pi}{8}} \qquad f_1 \approx \frac{1}{2}\frac{1}{|J_b/\overline{h}|}\sqrt{\frac{\pi}{8}} \exp\left(-\frac{1}{8}(\overline{h}\omega_0/J_b)^2\right) \tag{A18}$$

so equation (A12) becomes

$$\Delta B_{1/2} = \frac{1}{\gamma_e}\frac{(\mu_B B_0)^2}{\overline{h}|J_b|}\sqrt{\frac{\pi}{8}}\,\mathrm{Re}\left(|\Delta g_{zz}|^2 + |\Delta g_{zx} + \mathrm{i}\,\Delta g_{zy}|^2 \frac{1}{2} \exp\left[-\frac{1}{8}(\overline{h}\omega_0/J_b)^2\right]\right) \tag{A19}$$

which is used to analyse the contribution of the anisotropic Zeeman interaction to the ESR linewidth.

References

[1] Nojiri H, Shimamoto Y, Miura N, Hase M, Uchinokura K, Kojima H, Tanaka I and Shibuya Y 1995 *Phys. Rev.* B **52** 12 749

[2] Nishi M, Fujita O and Akimitsu J 1994 *Phys. Rev.* B **50** 6508

[3] Hase M, Terasaki I, Uchinokura K, Tokunaga M, Miura N and Obara H 1993 *Phys. Rev.* B **48** 9616

[4] Bray J W, Jacobs I S, Interrante L V and Bonner J C 1982 *Extended Linear Chain Compounds* vol 2, ed J S Miller (New York: Plenum) p 353

[5] Hirota K, Cox D E, Lorenzo J E, Shirane G, Tranquada J M, Hase M, Uchinokura K, Kojima H, Shibuya Y and Tanaka I 1994 *Phys. Rev. Lett.* **73** 736

[6] van Loosdrecht P H M, Boucher J P, Martinez G, Dhalenne G and Revcolevschi A 1996 *Phys. Rev. Lett.* **76** 311

[7] Dević S D, Konstantinović M J, Pović Z V, Dhalenne G and Revcolevschi A 1994 *J. Phys.: Condens. Matter* **6** L745

[8] Liu X, Wosnitza J, von Löhneysen H and Kremer R K 1995 *Phys. Rev. Lett.* **75** 771

[9] Hori H, Furusawa M, Sugai S, Honda M, Takeuchi T and Kindo K 1995 *Physica* B **211** 180

[10] Oseroff S, Cheong S-W, Fondado A, Aktas B and Fisk Z 1994 *J. Appl. Phys.* **75** 6819

[11] Brill T M, Boucher J P, Voiron J, Dhalenne G, Revcolevschi A and Renard J P 1994 *Phys. Rev. Lett.* **73** 1545

[12] Yamada I, Nishi M and Akimitsu J 1996 *J. Phys.: Condens. Matter* **8** 2625

[13] Honda M, Shibata T, Kindo K, Sugai S, Takeuchi T and Hori H 1996 *J. Phys. Soc. Japan* **65** 691

[14] Ohta H, Imagawa S, Yamamoto Y, Motokawa M, Fujita O and Akimitsu J 1994 *J. Magn. Magn. Mater.* **140–144** 1685

[15] Palme W, Ambert G, Boucher J P, Dhalenne G and Revcolevschi A 1996 *Phys. Rev. Lett.* **76** 4817

[16] Muller F, Hopkins M A, Coron N, Grynberg M, Brunel L C and Martinez G 1989 *Rev. Sci. Instrum.* **60** 3681

[17] Völlenkle H, Wittmann A and Nowotny H 1967 *Monatsh. Chem.* **98** 1352
[18] Kubo R and Tomita K 1954 *J. Phys. Soc. Japan* **9** 888
[19] Kubo R 1962 *Fluctuation, Relaxation and Resonance in Magnetic Systems* ed D ter Haar (New York: Plenum)
[20] Richards P M 1976 *Scuola Internazionale di Fisica Enrico Fermi* vol 59, ed K A Müller and A Rigamonti (Amsterdam: North-Holland) p 539
[21] Date M, Yamazaki H, Motokawa M and Tazawa S 1970 *Suppl. Prog. Theor. Phys.* **46** 194
[22] Moriya T 1969 *Phys. Rev.* **120** 91
[23] Bencini A and Gatteschi D 1990 *Electron Paramagnetic Resonance of Exchange Coupled Systems* (Berlin: Springer)